This is a preprint, the final version is subject to change, of the American Mineralogist (MSA)
Cite as Authors (Year) Title. American Mineralogist, in press.
(DOI will not work until issue is live.) DOI: http://dx.doi.org/10.2138/am.2013.4462

Revision # 1

Compressibility and structural stability of two variably hydrated olivine samples ($Fo_{97}Fa_3$) to 34 GPa by X-Ray diffraction and Raman spectroscopy

Murli H. Manghnani,[1] Anwar Hushur,[1,2] Joseph R. Smyth,[3] Fabrizio Nestola,[4] Przemyslaw Dera[5] , Mariappan Sekar[6], George Amulele [1,7], Daniel J. Frost [8]

[1]University of Hawaii, Hawaii Institute of Geophysics and Planetology, Honolulu, HI 96822, USA (murli@soest.hawaii.edu)

[2]Present address: School of Physics Science and Technology, Xinjiang University, Urumqi, 830046, P. R. China

[3]Department of Geological Sciences, University of Colorado, Boulder, CO 80309, USA

[4]Department of Geosciences, University of Padova, Via Gradenigo 6, I-35131, Padova, Italy

[5] Center for Advanced Radiation Sources, The University of Chicago, Argonne National Laboratory University of Chicago, Chicago, IL 60637, USA

[6]Present address: Indira Gandhi Center for Atomic Research, Kalpaakam 603 102, Tamil Nadu, India

[7]Present address: Department of Geology and Geophysics, Yale University, New Haven CT 06520, USA

[8]Bayerisches Geoinstitut, Universität Bayreuth, 95440, Bayreuth, Germany

ABSTRACT

Two hydrous olivines of composition $Fo_{97}Fa_3$ with water content of 4883 parts per million by weight (ppmw) (SZ0407A) and 8000 ppmw (SZ0407B) were synthesized at 1250 ºC and 12 GPa. Single-crystal X-ray diffraction was used to determine unit cell parameters of SZ0407A and SZ0407B at pressures up to 7.1 GPa at room temperature. Synchrotron powder X-ray diffraction and Raman scattering experiments were performed on sample SZ0407A in a diamond-anvil cell to 34 GPa at room temperature. For both samples, the compressibility is the largest along the *b*-axis and smallest along the *a*-axis. Using the compression (V/V_o) *vs.* pressure data for sample SZ0407A to 29.08 GPa, in conjunction with the third-order Birch-Murnaghan equation of state, we calculate the isothermal bulk modulus and its pressure derivative as K_o = 119.4(15) GPa and K'_o = 6.6(5). Single-crystal compression data for sample SZ0407A to 7 GPa give K_o = 121.5(6) GPa and K'_o = 5.7(2); and for sample SZ0407B K_o = 122.2(12) GPa and K'_o = 6.2(4). High-pressure Raman spectra for SZ0407A up to 34 GPa show a continuous shift of all the observed bands to higher frequency with increasing pressure; there is no indication of any first-order phase transition. However, the Raman spectra indicate subtle discontinuous changes around 22 GPa, unobserved in previously reported studies on anhydrous olivines.

Keywords: Hydrous olivine, X-ray diffraction, Raman spectroscopy, hydration mechanism, high pressure

INTRODUCTION

The nominally anhydrous mineral phases in the Earth's deep upper mantle and transition zone (410-660 km depth) may serve as a large internal reservoir of water that has profound implications for Earth's evolution as a water planet. Water plays important roles in the phase transformation kinetics in the Earth's interior, which affects the mantle dynamics (e.g. Kubo et al. 1998). Trace or minor hydroxyl in these phases affects strength and rheology (Chen et al. 1998; Kavner 2003; Mei and Kohlstedt 2000), and electrical conductivity (Poe et al. 2010). Therefore, it is important to understand the state of water and its role in the structure of minerals in the Earth's interior. Much effort has been put into estimating the OH^- storage capacity of nominally anhydrous mineral phases to determine factors controlling OH^- incorporation into the structure (Bai and Kohlstedt 1993; Bell et al. 2003; Hushur et al. 2009; Khisina et al. 2001; Kohlstedt et al. 1996; Mackwell and Kohlstedt 1990; Matveev et al. 2001; Miller et al. 1987; Mosenfelder et al. 2006; Rossman and Smyth 1990; Skogby et al. 1990; Smyth 1994; Walker et al. 2007). These studies have revealed that hydroxyl occurrence in nominally anhydrous mantle phases is closely related to cation vacancy defects. Although point defects have been linked to hydrogen incorporation, there remain several questions as to which point defect predominates under various P,T conditions.

Olivine $(Mg,Fe)_2SiO_4$ is the most abundant mineral phase in the upper mantle to a depth of 410 km, and it is nominally anhydrous. Although natural olivines typically contain less than 200 ppmw H_2O by weight, samples synthesized at pressures of 12-14 GPa have been obtained with up to 8900 ppmw, enough to significantly affect elastic and other physical properties (Litasov et al. 2007; Smyth and Jacobsen 2006) as well as the overall hydrogen budget of the planet. This has generated broad interest in systematic investigation of the various structural and elastic (seismic) properties, as well as the stability of these phases as a function of water content. X-ray diffraction (XRD) can give the full image of a crystal structure averaged over a sample volume; however information on local structural disorder,

dynamics and defects with small concentrations may be limited. In contrast, spectroscopy is very sensitive to the local structural disorder and defects. A combination of both XRD and spectroscopic studies may give important additional information on crystal structures such as disorder and dynamics, and may even help avoiding pitfalls in structure solution (Libowitzky 2006).

The XRD technique has been applied in various previous studies to understand the structure and compressibility of both hydrous and anhydrous olivines. Isothermal compression methods, deploying powder or single-crystal X-ray diffraction techniques, yield unit cell volume as a function of pressure (P-V relations) which enables calculation of isothermal bulk modulus (K_T) and its pressure derivative ($\partial K_T/\partial P$). The isothermal bulk modulus K_T is related to the adiabatic bulk modulus K_S by

$$K_s = K_T (1 + \alpha\gamma T),$$

where α is the thermal expansion coefficient (~2.6 x 10^{-5} K^{-1}) (Fei 1995; Kroll et al. 2012; Ye et al. 2009), γ is the Grüneisen parameter ($\approx$ 1) (Anderson 1989), and T is temperature (K). In general, K_s is roughly one to two percent larger than K_T. Table 1 summarizes elasticity data for anhydrous and hydrous olivines. One of the major findings is that the effect of hydration is to decrease bulk modulus (K_o) and increase K_o' by increasing the vacancy or unoccupied volume in the structure.

Anhydrous olivine has been widely studied by vibrational spectroscopies. The pressure dependencies of the Raman and IR spectra at room temperature have been measured in several studies for the end-members forsterite and fayalite, as well as for some intermediate compositions. Both Raman (Besson et al. 1982; Chopelas 1990; Durben et al. 1993; Gillet et al. 1991; Wang et al. 1993) and IR data (Hofmeister 1997; Hofmeister et al. 1989; Williams et al. 1990) show that the high frequency modes (> 500 cm^{-1}), related to the internal vibrations of the isolated SiO_4 tetrahedra of the olivine structure have smaller mode Grüneisen parameters than the lattice modes, which involve vibrations of the MgO_6 octahedra. This effect is consistent with the larger compressibility and relative weakness of the Mg-O bond compared to the Si-O bond as shown by high pressure x-ray diffraction studies (Hazen 1976; Kudoh and Takéuchi 1985), and discussed in detail by Smyth et al. (2000). Vibrational studies to date have not been carried out for Fe-bearing olivines with significant hydration. We report

here single-crystal XRD data up to 7.1 GPa, powder synchrotron XRD data up to ~29 GPa, and Raman spectroscopic data of synthesized hydrous $Fo_{97}Fa_3$ olivine samples in the diamond anvil cell up to 34 GPa. Raman spectra of high-quality single crystals of hydrous olivine were measured in the wide spectral range of 190 – 3700 cm^{-1}. Our aim was to investigate the effect of water on the compressibility and vibrational properties, the local structure of hydrous Fe-bearing olivine, and to track changes in H bonding and proton environments under pressure.

EXPERIMENTAL METHODS

Synthesis of these hydrous olivines was carried out in double-capsule experiments in the 5000-ton multi-anvil press at Bayerisches Geoinstitut at 12 GPa and 1250°C (Smyth et al. 2006). In these experiments, pyroxene-normative and periclase-normative compositions were formulated with about 3 weight percent H_2O. The two compositions were welded into separate inner Pt capsules and packed with brucite into a welded outer capsule. When the inner capsules were opened free liquid water emerged. The silica-excess capsule contained olivine, enstatite, and a small amount of apparent quench melt phase. The silica deficient capsule contained olivine, clinohumite and a quenched melt phase. The olivine, clinohumite and clinoenstatite were identified by Raman spectroscopy and by single crystal X-ray diffraction. The grain size of the silica excess sample was about 100 μm, whereas that of the silica deficient capsule was about 250 μm. H_2O contents were measured by polarized FTIR spectroscopy on X-ray-oriented, faceted single crystals. The contents were computed from integrated absorbances using the calibration of Bell et al. (2003) for olivine. Sample SZ0407A contained 4883 (±500) ppmw H_2O, whereas sample SZ0407B contained 8000 (±500) ppmw.

Unit-cell parameters were measured as a function of pressure up to 7.1 GPa by single-crystal X-ray diffraction. For the single crystal X-ray diffraction we used a steel gasket T-301 and methanol:ethanol 4:1 mixture was used as transmitting pressure, which is hydrostatic at least up to 9.4 GPa as demonstrated by Angel et al. (2007). The X-ray source was the MoKalpha with working conditions at 50 kV and 40 mA. Two crystals (SZ0407A and B) were loaded into the diamond cell along with a quartz crystal for an internal pressure standard. Cell parameters of the two crystals and quartz were measured at 13 different pressures up to 7.1 GPa using a Huber four-circle

diffractometer operating under the program SINGLE (Angel and Finger 2011). Pressures were determined using the quartz calibration curve of Angel et al. (1997).

High-pressure synchrotron powder X- ray diffraction studies in angle-dispersive mode on the hydrous olivine (SZ0407A) were carried out up to 29 GPa at the GeoSoilEnviroCARS beam line (13-BM-D) at the Advanced Photon Source (APS) using a monochromatic X-ray beam of energy of 37.07 keV (λ = 0.3344 Å). Finely powdered samples of grain size 1-3 μm were loaded in a piston-cylinder type diamond-anvil cell (DAC) of culet size 250 μm. We used a steel gasket T-301 and silicone oil was used as the pressure transmitting medium. The pressure was estimated using the shift in the R1 line of the ruby loaded along with the sample (Mao et al. 1986). The average time for measurement at each pressure was 10 minutes. Fit2D (Hammersley et al. 1996) was used to reduce the data to 2-theta *vs.* intensity profiles. The unit-cell parameters were estimated from the *d*-spacings at each pressure using the program Unit Cell (Holland and Redfern 1997). We have used the peaks (1 1 2), (1 3 0), (1 0 2), (0 2 1) and (0 2 0) for the lattice parameter calculation.

Raman spectra were recorded using a triple monochromator Dilor XY spectrometer equipped with a liquid nitrogen-cooled charge-coupled-device (CCD) detector. The 514.5 nm green line of an Ar ion laser from Spectra Physics was used to excite the sample. The laser light was focused using an OLYMPUS microscope with a long distance 50× objective to a spot of about 3 μm diameter in the sample with the laser power being 25 mW on the sample. No laser heating effects should occur under such conditions. The spectrometer was calibrated using single-crystal silicon as a reference. For high-pressure measurements in the diamond anvil cell, a rhenium gasket was pre-indented to 42 μm thickness and an 85 μm diameter hole was drilled at the center of the indentation. A randomly oriented single crystal fragment 35 × 40 × 20 μm^3 in size was mounted in a diamond-anvil cell where diamonds had 350 μm diameter culets. Two pieces of ruby ~5 μm in size were placed at the two sides of the sample for pressure calibration. Liquid argon was loaded as a pressure-transmitting medium using a liquid nitrogen cooling method. Pressure was estimated using the shift in the R1 line of the ruby loaded along with the sample (Mao et al. 1986). All spectra were recorded in the backscattering geometry with no polarization used for the collected signal.

RESULTS AND DISCUSSION

Unit cell parameters of hydrous Fo_{97} containing 4883 ppmw H_2O (SZ0407A) and hydrous Fo_{97} containing 8000 ppmw H_2O (SZ0407B) measured at ambient conditions and 12 pressures by single-crystal XRD are reported in Table 2. The measured pressure dependencies of the unit-cell volumes are plotted in Figures 1 and 2. The program EOSFIT5.2 (Angel 2002) was used to fit equation of state parameters to the observed compression data. The fitting is weighted according to the estimated error of pressure determination and fitting error of volume determination. The isothermal bulk modulus and its derivative were estimated using the third order Birch-Murnaghan equation of state.

$$P(V) = \frac{3K_o}{2}\left[\left(\frac{V_o}{V}\right)^{\frac{7}{3}} - \left(\frac{V_o}{V}\right)^{\frac{5}{3}}\right]\left\{1 + \frac{3}{4}\left(K_o' - 4\right)\left[\left(\frac{V_o}{V}\right)^{\frac{2}{3}} - 1\right]\right\}$$

where K_o is the bulk modulus at ambient pressure, K_o' is its first pressure derivative, and V_o is the reference volume. Single crystal data to 7.1 GPa give K_o = 121.5(6) GPa and K_o' = 5.7(2) for sample SZ0407A, and K_o = 122.2(12) GPa and K_o' = 6.2(4) for sample SZ0407B. The K_o and K_o' of SZ0407A and SZ0407B show that slightly different water content (~ 3200 ppmw) has minimal effect on the bulk modulus within experimental uncertainty. The values are K_o = 119.2(12) GPa and K_o' = 6.6(0.4) for combined single-crystal and powder diffraction data for sample SZ0407A, and no distinctive changes were observed in the isothermal volume compressibility. The compression data for all samples are thus in very good agreement and indicate a decrease of about 6 percent in bulk modulus relative to anhydrous forsterite data cited above. Comparison of bulk modulus of hydrous Fo_{97} containing 8000 ppmw H_2O with hydrous Fo_{95} containing 8000 ppmw H_2O (Smyth et al. 2005; Smyth and Jacobsen 2006) which is 120(2) GPa shows that the 2 mol% Fe has no effect on K_o within experimental uncertainty. Although we observe a decrease in bulk modulus with hydration, the effects of hydration on elasticity of forsterite may not be simple. Mao et al. (2010) report a crossover of the velocities of hydrous and anhydrous forsterite measured by Brillouin scattering at high pressure.

The axial compressibility is the largest along the *b* axis and smallest along the *a* axis as shown in Figure 3. The axial compression values were β_a = 0.00166(2), β_b = 0.00309(4), and β_c = 0.00243(3) GPa^{-1} for SZ0407A, respectively. For SZ0407B, the axial compression values were β_a = 0.00158(3), β_b = 0.00308(4), and β_c = 0.00240(3) GPa^{-1}. The *a*:*b*:*c* axial compressibility ratio was 1:1.9:1.5 for both SZ0407A and SZ0407B. The anisotropic nature of the compression is a common feature for all anhydrous olivines. The compression along the *b* axis depends on the compression of the most compressible structural unit, the M2 octahedron. Our result is consistent with studies on anhydrous olivines, with the *b* axis being the most compressible axis. However, our results also indicate an increase of the compressibility along the *a* and *c* axis as compared to the anhydrous forsterite and anhydrous olivine $Fo_{83}Fa_{17}$ (Andrault et al. 1995; Smyth et al. 2000; and references therein), which may be related to the hydration mechanism in hydrous olivine (SZ0407A, SZ0407B).

Raman spectra in the lattice and silicate vibrational region of hydrous olivine $Fo_{97}Fa_3$ containing 4883 ppmw water (SZ0407A) measured as a function of pressure to 34 GPa are shown in Figure 4. The ambient spectra are similar to those reported in previous Raman studies (Besson et al. 1982; Chopelas 1990, 1991; Durben et al. 1993; Gillet et al. 1991; Iishi 1978; Piriou and McMillan 1983; Wang et al. 1993). With increasing pressure, all the twelve observed modes show a continuous shift to higher frequency. Of these, four modes exhibit a linear pressure dependence of frequency; however the remaining eight modes are characterized by a nonlinear response. For these 8 modes, the frequency *vs.* pressure data were fitted with quadratic equations as shown in Figures 5 and 6. According to the original definition for a vibrational mode of frequency ν_i, a mode Grüneisen parameter is defined by

$$\gamma_i = -\frac{d\ln(\nu_i)}{d\ln(V)}$$

where *V* is volume. γ_i were determined by fitting $\ln(\nu_i)$ versus $\ln(V)$ values linearly, and are shown in Table 3. γ_i of the mode related to $Mg(2)O_6$ translation (Table 3) does not show marked changes in hydrous olivine $Fo_{97}Fa_3$ (SZ0407A) relative to anhydrous forsterite. γ_i of all the observed modes related to SiO_4 tetrahedra show an increase as compared to those for anhydrous forsterite, indicating Si-O bonds in hydrous olivine $Fo_{97}Fa_3$ (SZ0407A) are more compressible than Si-O bonds in anhydrous olivine. This may be responsible for the increase of the compressibility along the *a* and *c* axis as compared to the anhydrous forsterite and

anhydrous olivine $Fo_{83}Fa_{17}$ (Andrault et al. 1995; Smyth et al. 2000; and references therein). Our Raman study on Fe-free hydrous forsterite does not show such an increase in γ_i of the modes related to SiO_4 tetrahedra (Hushur et al. 2009), which may indicate that the hydration mechanism is different in hydrous olivine $Fo_{97}Fa_3$ (SZ0407A) as compared to the hydrous forsterite. May be, a significant protonation of Si-vacancies also exist in this hydrous olivine $Fo_{97}Fa_{3..}$

In the entire pressure range of this study, the sharp Raman bands assigned to vibrations of the olivine crystal structure are retained, indicating no evidence of any phase transition. However, the high-pressure spectra do indicate some subtle structural modification. Specifically, in the low frequency spectra range between 200 cm^{-1} and 800 cm^{-1}, the M2 translation mode at 302.5 cm^{-1}, SiO_4 rotation mode at 325.2 cm^{-1} and ν_4 mode at 542.3 cm^{-1} disappears, whereas the ν_4 mode at 606.9 cm^{-1} intensifies in the high pressure Raman spectra as shown in Figure 5. Both 542.3 cm^{-1} and 606.9 cm^{-1} modes are initially A_g modes and represent anti-symmetric bending of the oxygens in SiO_4 tetrahedra. The disappearance of the 542.3 cm^{-1} mode above 22 GPa, while the mode at 606.9 cm^{-1} is intensified, is not an effect of sample orientation. This may indicate that the two bands represent vibrations of different structural units that appear or disappear above 22 GPa. Interestingly, the similarity of the high-pressure spectra with those of γ-spinel becomes more pronounced at high pressures: an intense band with a zero pressure location near 600 cm^{-1}, and a doublet at higher frequencies (Chopelas et al. 1994; Kleppe et al. 2002). The decrease in number of the Raman active modes at high pressure may indicate that the olivine structure is modified locally above 22 GPa, with the partial appearance of Si-O-Si linkages accompanied by a possible metastable increase in the silicon coordination. In our recent Raman study on Fe-free hydrous forsterite we observed a change in the pressure derivatives of many of the observed Raman modes at ~20 GPa (Hushur et al. 2009). However, in the current study on Fe-bearing hydrous forsterite we do not observe such a slope change at ~20 GPa. This may be related to different local environments in Fe-bearing hydrous forsterite as compared to the Fe-free hydrous forsterite.

The olivine structure is orthorhombic containing isolated SiO_4 units linked by octahedrally coordinated divalent cations. The divalent cations are in two crystallographically distinct sites, the smaller M1 (C_i symmetry) site and larger M2 (C_s symmetry) site. The Ml octahedron shares six edges with neighboring polyhedra, two with SiO_4 tetrahedra. The M2

263 octahedra share three edges with neighboring polyhedra but only one with a SiO_4 tetrahedron.
264 The unit cell parameters increase in Fe-bearing hydrous forsterite as compared to the Fe-free
265 hydrous forsterite that has the same amount of hydrogen present. Kudoh et al. (2006) and
266 Kudoh et al. (2007) reported on a single-crystal X-ray structural analysis of Fe-bearing
267 ($Mg_{1.85}Fe_{0.14}Si_{0.99}H_{0.06}O_4$) and Fe-Free ($Mg_{1.985}Si_{0.993}H_{0.06}O_4$) hydrous forsterite, in which
268 increases in the *a*, *b*, and *c* axes due to the effect of Fe were 0.13%, 0.08%, and 0.03%,
269 respectively, and showing a 0.2 % increase in the unit cell volume due to the presence of Fe.
270 In Fe-bearing hydrous forsterite, cation vacancies predominantly occurred at the M2 site
271 (Kudoh 2008; Kudoh et al. 2007), in contrast to the case of Fe-free hydrous forsterite in which
272 the cation vacancies predominantly occur at the M1 site (Hushur et al. 2009; Kudoh 2008;
273 Kudoh et al. 2006; Smyth et al. 2006). A vacancy at the M1 site leads to an increase in the
274 M2-O bond length in Fe-free hydrous forsterite. In case of the Fe-bearing hydrous forsterite,
275 Fe atoms lead to an increase in both the M1-O and M2-O bond lengths. The difference in
276 proton occupancy between Fe-bearing hydrous forsterite and the Fe-free hydrous forsterite
277 may be responsible for the different pressure dependence of the Raman modes observed in the
278 Fe-bearing hydrous forsterite as compared to the Fe-free hydrous forsterite.
279 The Raman modes of the hydroxyl groups in hydrous olivine (SZ0407A) are shown in
280 Figure 7. We fit the observed spectra at ambient pressure by four Gaussian functions using
281 ORIGIN Pro 7.5 software. The spectra above 9 GPa are fitted with three Gaussian functions.
282 The mode frequency as a function of pressure obtained by fitting is shown in Figure 8. At
283 ambient pressure, four Raman bands were observed at 3555, 3578, 3613, and 3656 cm^{-1}. It is
284 similar to the FTIR spectra measured on the sample SZ0407B and SZ0408A (Smyth et al.
285 2006), and Raman spectra of the sample SZ408A (Hushur et al. 2009). However, an
286 additional Raman mode at 3656 cm^{-1} is observed only on this hydrous olivine (SZ407A). As
287 pressure increases, the Raman active OH stretching modes of hydrous olivine (SZ0407A)
288 with frequencies < 3600 cm^{-1} have strong, negative pressure dependence whereas OH modes
289 at higher frequencies are less sensitive to pressure. According to the empirical relation
290 between OH-stretching frequencies and O···O distances (Libowitzky 1999), a negative
291 frequency response of OH modes under pressure requires a reduction of the respective O···O
292 distances and indicates a strengthening of the hydrogen bond.

The protonation of hydrous olivine has been studied extensively by FTIR spectroscopy. Previous studies show that there are two different mechanisms related to silicon and magnesium vacancies by which hydrogen is incorporated into olivine crystal structure. Bai and Kohlstedt (1993) and Kohlstedt et al. (1996) suggested protonation of Mg-vacancies in the olivine structure, whereas Litasov et al. (2009), Matveev et al. (2001) and Lemaire et al. (2004) preferred significant protonation of Si-vacancies. Assuming linear O-H…O topologies, we can correlate the observed OH stretching frequencies with O…O bond distances (Libowitzky 1999). Octahedral edges in the olivine structure range from 2.85 to 3.33 Å except for edges shared with the tetrahedron, which are about 2.55 Å. Tetrahedral edges range from 2.55 to 2.76 Å. The largest and broad peak in the pattern at 3555 cm^{-1} (in the *b*-direction) is consistent with protonation of the shared O3-O3 edges (2.76 Å) of the M2 octahedron. The mode at 3578 cm^{-1} could correspond to the unshared O1-O3 edge of M1 (2.84 Å). The peak at 3613 cm^{-1} corresponds to protonation of an O-O distance of > 2.8 Å (Libowitzky 1999), and is consistent with the O1-O2 edge shared between M1 octahedra (2.85Å). There is also the possibility of the O3-O3 edge of the M2 octahedron (2.99 Å), but a proton on this edge would require a strongly bent O-H…O angle to be consistent with polarizations. The mode at 3656 cm^{-1} corresponds to protonation of an O-O distance of > 2.9 Å (Libowitzky 1999) and is consistent with the O3-O3 edge of the M2 octahedron (2.99 Å) in this Fe-bearing olivine. There might be significant deviations from the linear O-H…O topologies, or the stretching mode at 3656 cm^{-1} is not from the hydrogen bonded O-H group. Khisina et al. (2001) reported an OH band at 3656 cm^{-1} which is related to the 10 Angstrom phase. However the strong intensity of this band in our spectra indicates that it is not from the minor phases in olivine. And also the single crystal data of our synthetic sample did not show any monoclinic phase in our studied sample. Therefore, it is not likely from the 10 Angstrom phase. May be the band at 3656 cm^{-1} is related to the Si vacancies. The band at 3656 cm^{-1} shows splitting into two modes above 15 GPa and this may be related to the observed local structural modification in this study. It would be enlightening to carry out complementary FTIR measurements on such a hydrous olivine sample. The above initial findings may aid in refining the models for structural stability and compressibility (seismic velocities) of hydrous phases in the upper mantle.

ACKNOWLEDGMENTS

We thank Professor Quentin Williams for helpful comments for improving the manuscript. Thanks are due to John Balogh for maintaining the Raman system in good working order. This work was supported by US National Science Foundation grants EAR 0538884 and 0957137 to MHM, and EAR 11-13369 to JRS. Syntheses were performed at Bayerisches Geoinstitut, Universitaet Bayreuth, Germany, and supported, in part, by the Alexander von Humboldt Foundation to JS and FN. Portions of this work were performed at GeoSoilEnviroCARS (Sector 13), Advanced Photon Source (APS), Argonne National Laboratory. GeoSoilEnviroCARS is supported by the National Science Foundation - Earth Sciences (EAR-1128799) and Department of Energy - Geosciences (DE-FG02-94ER14466). Use of the Advanced Photon Source was supported by the U. S. Department of Energy, Office of Science, Office of Basic Energy Sciences, under Contract No. DE-AC02-06CH11357. The SOEST and HIGP contribution numbers for this paper are xxxx and xxxx.

REFERENCES CITED

Abramson, E., Brown, J., Slutsky, L., and Zaug, J. (1997) The elastic constants of San Carlos olivine to 17 GPa. Journal of Geophysical Research, 102(B6), 12253-12263.

Anderson, D.L. (1989) Theory of the Earth. Blackwell, Boston.

Andrault, D., Bouhifd, M., Itie, J., and Richet, P. (1995) Compression and amorphization of $(Mg, Fe)_2SiO_4$ olivines: An X-ray diffraction study up to 70 GPa. Physics and Chemistry of Minerals, 22(2), 99-107.

Angel, R.J. (2002) EOSFIT V5. 2 program. Crystallography Laboratory, Virginia Tech, Blacksburg, USA.

Angel, R.J., Allan, D., Miletich, R., and Finger, L. (1997) The use of quartz as an internal pressure standard in high-pressure crystallography. Journal of Applied Crystallography, 30(4), 461-466.

Angel, R.J., Bujak, M., Zhao, J., Gatta, G.D., and Jacobsen, S.D. (2007) Effective hydrostatic limits of pressure media for high-pressure crystallographic studies. Journal of Applied Crystallography, 40, 26-32.

Angel, R.J., and Finger, L.W. (2011) SINGLE: a program to control single-crystal diffractometers. Journal of Applied Crystallography, 44(1), 247-251.

Bai, Q., and Kohlstedt, D.L. (1993) Effects of chemical environment on the solubility and incorporation mechanism for hydrogen in olivine. Physics and Chemistry of Minerals, 19(7), 460-471.

Beran, A., and Libowitzky E. (2006) Water in natural mantle minerals II: Olivine, garnet and accessory minerals. Reviews in Mineralogy and Geochemistry, 62,169-191.

Bass, J.D. (1995) Elasticity of minerals, glasses, and melts. AGU Reference Shelf, 2, 45-63.

Bell, D.R., Rossman, G.R., Maldener, J., Endisch, D., and Rauch, F. (2003) Hydroxide in olivine: A quantitative determination of the absolute amount and calibration of the IR spectrum. Journal of Geophysical Research-Solid Earth, 108(B2), 2105.

Besson, J., Pinceaux, J., Anastopoulos, C., and Velde, B. (1982) Raman spectra of olivine up to 65 kilobars. Journal of Geophysical Research, 87(B13), 10773-10,775.

Chen, J., Inoue, T., Weidner, D.J., Wu, Y., and Vaughan, M.T. (1998) Strength and water weakening of mantle minerals, olivine, wadsleyite and ringwoodite. Geophysical Research Letters, 25(4), 575-578.

373 Chopelas, A. (1990) Thermal properties of forsterite at mantle pressures derived from
374 vibrational spectroscopy. Physics and Chemistry of Minerals, 17(2), 149-156.
375 -. (1991) Single crystal Raman spectra of forsterite, fayalite, and monticellite. American
376 Mineralogist, 76(7-8), 1101-1109.
377 Chopelas, A., Boehler, R., and Ko, T. (1994) Thermodynamics and behavior of γ-Mg_2SiO_4 at
378 high pressure: Implications for Mg_2SiO_4 phase equilibrium. Physics and Chemistry of
379 Minerals, 21(6), 351-359.
380 Downs, R.T., Zha, C.S., Duffy, T.S., and Finger, L.W. (1996) The equation of state of
381 forsterite to 17.2 GPa and effects of pressure media. American Mineralogist, 81(1),
382 51-55.
383 Durben, D.J., McMillan, P.F., and Wolf, G.H. (1993) Raman study of the high-pressure
384 behavior of forsterite (Mg_2SiO_4) crystal and glass. American Mineralogist, 78(11-12),
385 1143-1148.
386 Fei, Y. (1995) Thermal expansion. 29-44 p. American Geophysical Union Reference shelf 2,
387 Washington, D.C.
388 Gillet, P., Richet, P., Guyot, F., and Fiquet, G. (1991) High temperature thermodynamic
389 properties of forsterite. Journal of Geophysical Research-Solid Earth and Planets,
390 96(B7), 11805-11816.
391 Hammersley, A.P., Svensson, S.O., Hanfland, M., Fitch, A.N., and Hausermann, D. (1996)
392 Two-dimensional detector software: from real detector to idealised image or two-theta
393 scan. International Journal of High Pressure Research, 14(4-6), 235-248.
394 Hazen, R. (1976) Effects of temperature and pressure on the crystal structure of forsterite.
395 American Mineralogist, 61(11-12), 1280-1293.
396 Hofmeister, A.M. (1997) Infrared reflectance spectra of fayalite, and absorption data from
397 assorted olivines, including pressure and isotope effects. Physics and Chemistry of
398 Minerals, 24(7), 535-546.
399 Hofmeister, A.M., Xu, J., Mao, H.K., Bell, P.M., and Hoering, T.C. (1989) Thermodynamics
400 of Fe-Mg olivines at mantle pressures: Mid-and far-infrared spectroscopy at high
401 pressure. American Mineralogist, 74, 281-306.
402 Holland, T.J.B., and Redfern, S.A.T. (1997) Unit cell refinement from powder diffraction
403 data; the use of regression diagnostics. Mineralogical Magazine, 61(1), 65-77.

Hushur, A., Manghnani, M.H., Smyth, J.R., Nestola, F., and Frost, D.J. (2009) Crystal chemistry of hydrous forsterite and its vibrational properties up to 41 GPa. American Mineralogist, 94(5-6), 751-760.

Iishi, K. (1978) Lattice dynamics of forsterite. American Mineralogist, 63(11-12), 1198-1208.

Jacobsen, S.D., Jiang, F., Mao, Z., Duffy, T.S., Smyth, J.R., Holl, C.M., and Frost, D.J. (2008) Effects of hydration on the elastic properties of olivine. Geophysical Research Letters, 35(14), L14303.

-. (2009) Correction to "Effects of hydration on the elastic properties of olivine". Geophysical Research Letters, 36(12), L12302.

Kavner, A. (2003) Elasticity and strength of hydrous ringwoodite at high pressure. Earth and Planetary Science Letters, 214(3), 645-654.

Khisina, N.R., Wirth, R., Andrut, M., and Ukhanov, A.V. (2001) Extrinsic and intrinsic mode of hydrogen occurrence in natural olivines: FTIR and TEM investigation. Physics and Chemistry of Minerals, 28(5), 291-301.

Kleppe, A.K., Jephcoat, A.P., and Smyth, J.R. (2002) Raman spectroscopic study of hydrous gamma-Mg_2SiO_4 to 56.5 GPa. Physics and Chemistry of Minerals, 29(7), 473-476.

Kohlstedt, D.L., Keppler, H., and Rubie, D.C. (1996) Solubility of water in the alpha, beta and gamma phases of $(Mg,Fe)_2SiO_4$. Contributions to Mineralogy and Petrology, 123(4), 345-357.

Kroll, H., Kirfel, A., Heinemann, R., and Barbier, B. (2012) Volume thermal expansion and related thermophysical parameters in the Mg, Fe olivine solid-solution series. European Journal of Mineralogy, 24(6), 935-956.

Kubo, T., Ohtani, E., Kato, T., Shinmei, T., and Fujino, K. (1998) Effects of water on the α-β transformation kinetics in San Carlos olivine. Science, 281(5373), 85-87.

Kudoh, Y. (2008) Crystal structural features of hydrous forsterite: Effect of Fe on the M-site vacancies, possible hydrogen positions and variation of the unit cell dimensions. Journal of Mineralogical and Petrological Sciences, 103(5), 371-375.

Kudoh, Y., Kuribayashi, T., Kagi, H., and Inoue, T. (2006) Cation vacancy and possible hydrogen positions in hydrous forsterite, $Mg_{1.985}Si_{0.993}H_{0.06}O_4$, synthesized at 13.5 GPa and 1300 ^oC. Journal of Mineralogical and Petrological Sciences, 101(5), 265-269.

Kudoh, Y., Kuribayashi, T., Litasov, K., and Ohtani, E. (2007) Cation vacancies and possible hydrogen atom positions in Fe-bearing hydrous forsterite, $Mg_{1.85}Fe_{0.14}Si_{0.99}H_{0.06}O_4$, synthesized at 13.5 GPa and 1400 ^{o}C. Journal of Mineralogical and Petrological Sciences, 102(5), 306-310.

Kudoh, Y., and Takéuchi, Y. (1985) The crystal structure of forsterite Mg_2SiO_4 under high pressure up to 149 kb. Zeitschrift für Kristallographie, 171(3-4), 291-302.

Lemaire, C., Kohn, S.C., and Brooker, R.A. (2004) The effect of silica activity on the incorporation mechanisms of water in synthetic forsterite: a polarised infrared spectroscopic study. Contributions to Mineralogy and Petrology, 147(1), 48-57.

Libowitzky, E. (1999) Correlation of O-H stretching frequencies and O-H…O hydrogen bond lengths in minerals. Monatshefte Für Chemie, 130(8), 1047-1059.

-. (2006) Crystal structure dynamics: Evidence by diffraction and spectroscopy. Croatica chemica acta, 79(2), 299-309.

Litasov, K., Shatskiy, A., Katsura, T., and Ohtani, E. (2009) Water solubility in forsterite at 8–14 GPa. Doklady Earth Sciences, 425, 432-435.

Litasov, K.D., Ohtani, E., Kagi, H., Jacobsen, S.D., and Ghosh, S. (2007) Temperature dependence and mechanism of hydrogen incorporation in olivine at 12.5–14.0 GPa. Geophysical Research Letters, 34(16), L16314.

Mackwell, S.J., and Kohlstedt, D.L. (1990) Diffusion of hydrogen in olivine: implications for water in the mantle. Journal of Geophysical Research, 95(B4), 5079-5088.

Mao, H., Xu, J., and Bell, P. (1986) Calibration of the ruby pressure gauge to 800 kbar under quasi-hydrostatic conditions. Journal of Geophysycal Research, 91(B5), 4673-4676.

Mao, Z., Jacobsen, S.D., Jiang, F., Smyth, J.R., Holl, C.M., Frost, D.J., and Duffy, T.S. (2010) Velocity crossover between hydrous and anhydrous forsterite at high pressures. Earth and Planetary Science Letters, 293(3–4), 250-258.

Matveev, S., O'Neill, H.S., Ballhaus, C., Taylor, W.R., and Green, D.H. (2001) Effect of silica activity on OH-IR spectra of olivine: Implications for low-αSiO_2 mantle metasomatism. Journal of Petrology, 42(4), 721-729.

Mei, S., and Kohlstedt, D.L. (2000) Influence of water on plastic deformation of olivine aggregates 1. Diffusion creep regime. Journal of Geophysical Research-Solid Earth, 105(B9), 21457-21469.

Miller, G.H., Rossman, G.R., and Harlow, G.E. (1987) The natural occurrence of hydroxide in olivine. Physics and Chemistry of Minerals, 14(5), 461-472.

Mosenfelder, J.L., Deligne, N.I., Asimow, P.D., and Rossman, G.R. (2006) Hydrogen incorporation in olivine from 2-12 GPa. American Mineralogist, 91(2-3), 285-294.

Piriou, B., and McMillan, P. (1983) The high-frequency vibrational spectra of vitreous and crystalline orthosilicates. American Mineralogist, 68(3-4), 426-443.

Poe, B.T., Romano, C., Nestola, F., and Smyth, J.R. (2010) Electrical conductivity anisotropy of dry and hydrous olivine at 8 GPa. Physics of the Earth and Planetary Interiors, 181(3-4), 103-111.

Rossman, G.R., and Smyth, J.R. (1990) Hydroxyl contents of accessory minerals in mantle eclogites and related rocks. American Mineralogist, 75(7-8), 775-780.

Skogby, H., Bell, D.R., and Rossman, G.R. (1990) Hydroxide in pyroxene; variations in the natural environment. American Mineralogist, 75(7-8), 764-774.

Smyth, J.R. (1994) A crystallographic model for hydrous wadsleyite (β-Mg_2SiO_4): An ocean in the Earth's interior? American Mineralogist, 79(9-10), 1021-1024.

Smyth, J.R., Frost, D.J., and Nestola, F. (2005) Hydration of olivine and the Earth's deep water cycle. Geochimica et Cosmochimica Acta Supplement, 69, 746.

Smyth, J.R., Frost, D.J., Nestola, F., Holl, C.M., and Bromiley, G. (2006) Olivine hydration in the deep upper mantle: Effects of temperature and silica activity. Geophysical Research Letters, 33(15), L15301.

Smyth, J.R., and Jacobsen, S.D. (2006) Nominally anhydrous minerals and Earth's deep water cycle. In S. D. Jacobsen and S. van der Lee, Eds., Earth's Deep Water Cycle, Geophys. Monogr. Ser., 168 , p. 1–11, AGU, Washington, D. C.

Smyth, J.R., Jacobsen, S.D., and Hazen, R.M. (2000) Comparative crystal chemistry of orthosilicate minerals. Reviews in Mineralogy and Geochemistry, 41(1), 187-209.

Walker, A., Hermann, J., Berry, A., and O'Neill, H.S.C. (2007) Three water sites in upper mantle olivine and the role of titanium in the water weakening mechanism. Journal of Geophysical Research, 112(B5), B05211.

Wang, S.Y., Sharma, S.K., and Cooney, T.F. (1993) Micro-Raman and infrared spectral study of forsterite under high pressure. American Mineralogist, 78(5-6), 469-476.

Will, G., Hoffbauer, W., Hinze, E., and Lauterjung, J. (1986) The compressibility of forsterite up to 300 kbar measured with synchrotron radiation. Physica B & C, 139, 193-197.

Williams, Q., Knittle, E., Reichlin, R., Martin, S., and Jeanloz, R. (1990) Structural and electronic properties of Fe_2SiO_4-fayalite at ultrahigh pressures: Amorphization and gap closure. Journal of Geophysical Research, 95(B13), 21549-21563.

Ye, Y., Schwering, R.A., and Smyth, J.R. (2009) Effects of hydration on thermal expansion of forsterite, wadsleyite, and ringwoodite at ambient pressure. American Mineralogist, 94(7), 899-904.

Zha, C., Duffy, T.S., Downs, R.T., Mao, H., and Hemley, R.J. (1998) Brillouin scattering and X-ray diffraction of San Carlos olivine: direct pressure determination to 32 GPa. Earth and Planetary Science Letters, 159(1), 25-33.

509 # Table and Figure Captions

510

511 Table 1. Elastic properties of olivines.

512 Table 2. Unit-cell parameters of hydrous olivine $Fo_{97}Fa_3$ containing 4883 ppmw water
513 (SZ0407A) and hydrous olivine $Fo_{97}Fa_3$ containing 8000 ppmw water (SZ0407B) as
514 a function of pressure as determined by single-crystal X-ray diffraction.

515 Table 3. Mode frequencies (in cm^{-1}), mode Grüneisen parameters, and mode assignments for
516 observed Raman modes of hydrous olivine $Fo_{97}Fa_3$ containing 4883 ppmw water
517 (SZ0407A), and of anhydrous forsterite.

518 Figure 1. Unit-cell volumes of hydrous olivine $Fo_{97}Fa_3$ containing 4883 ppmw water
519 (SZ0407A, open squares) and hydrous olivine $Fo_{97}Fa_3$ containing 8000 ppmw water
520 (SZ0407B, open circles) as a function of pressure obtained from single-crystal XRD
521 studies. Error bars are also shown in the Figure. Solid and dashed lines represent the
522 two best-fit equations of state.

523 Figure 2. Unit-cell volumes of hydrous olivine $Fo_{97}Fa_3$ containing 4883 ppmw water
524 (SZ0407A) as a function of pressure. Open symbols represent powder XRD data.
525 Solid symbols are single-crystal XRD data. Solid and dashed lines represent the two
526 best-fit equations of state, based on powder and single-crystal XRD, and single-crystal
527 XRD, respectively. Note that the symbols are larger than the uncertainties.

528 Figure 3. Axial compressions a/a_o, b/b_o and c/c_o as a function of pressure for a hydrous
529 olivine $Fo_{97}Fa_3$ containing 4883 ppmw water (SZ0407A) and for hydrous olivine $Fo_{97}Fa_3$
530 containing 8000 ppmw water (SZ0407B). Note that the symbols are larger than the
531 uncertainties.

532 Figure 4. Raman spectra of hydrous olivine $Fo_{97}Fa_3$ containing 4883 ppmw water (SZ0407A)
533 to 33.9 GPa.

534 Figure 5. Pressure dependences of the observed low frequency Raman modes for hydrous
535 olivine $Fo_{97}Fa_3$ containing 4883 ppmw water (SZ0407A) from 200 ~ 750 cm^{-1}.

536 Figure 6. Pressure dependences of the four high frequency Raman modes for hydrous olivine
537 $Fo_{97}Fa_3$ containing 4883 ppmw water (SZ0407A) from 800 ~ 1200 cm^{-1}.

Figure 7. Pressure dependence of Raman spectra of hydrous olivine $Fo_{97}Fa_3$ containing 4883 ppmw water (SZ0407A) in the OH-stretching region. The spectra are offset for clarity. The solid red line in the 1 bar spectrum is a fit using four Gaussian functions. Labels at right side indicate pressure in gigapascals and numbers on the 1 bar spectrum indicate O-H stretching mode frequencies obtained from the fit.

Figure 8. Pressure dependence of the Raman modes of hydroxyl group in hydrous olivine $Fo_{97}Fa_3$ containing 4883 ppmw water (SZ0407A).

Tables and Figures

Table 1. Elastic properties of olivines

Olivine composition	Method	Pressure range (GPa)	K_s (GPa)	K_s'	K_T (GPa)	K_T'	References
Anhydrous							
Forsterite (Fo_{100})	Brillouin spectroscopy	32	129	4.2			Zha et al. (1998)
Forsterite (Fo_{100})		Ambient pressure	129.5				Bass (1995)
$Fo_{91}Fa_9$	Ultrasonic	3 GPa	129.5	4.65			Bass (1995)
$Fo_{93}Fa_7$		Ambient pressure	129.4				Bass (1995)
$Fo_{91.3}Fa_{8.7}$		Ambient pressure	128.1				Bass (1995)
$Fo_{92}Fa_8$		Ambient pressure	126.7				Bass (1995)
San Carlos olivine Fo_{90}	Impulsive-stimulated scattering	12	129.4(5)	4.29	126.3	4.28	Abramson et al. (1997)
Forsterite (Fo_{100})	Single-crystal XRD	17.2			125(2)	4.0(4)	Downs et al. (1996)
Forsterite (Fo_{100})	Single-crystal XRD	15			122.6	4.3	Kudoh and Takéuchi (1985)
Forsterite (Fo_{100})	Powder Synchrotron XRD	30			135.7(10)	3.9(10)	Will et al. (1986)
Hydrous							
Fo_{95} (8000 ppmw H_2O)	Single-crystal XRD	8			120(2)		Smyth et al. (2005)
Fo_{100} (0.8-0.9 wt% H_2O)	Brillouin scattering		125.7(2)				Jacobsen et al. (2008, 2009)
Fo_{97} (0.8-0.9 wt% H_2O)	Brillouin scattering		125.2(8)				Jacobsen et al. (2008, 2009)
$Fo_{97}Fa_3$ (4883 ppmw H_2O)	Single-crystal XRD	7			121.5(6)	5.7(2)	This study
$Fo_{97}Fa_3$ (8000 ppmw H_2O)	Single-crystal XRD	7			122.2(12)	6.3(10)	This study

Table 2. Unit cell parameters of hydrous olivines SZ0407A and SZ0407B as a function of pressure as determined by single-crystal X-ray diffraction.

Pressure(GPa)	SZ0407A					SZ0407B				
P(GPa)	*a*(Å)	*b*(Å)	*c*(Å)	V(Å^3)	V/Vo	*a*(Å)	*b*(Å)	*c*(Å)	V(Å^3)	V/Vo
0.0001	4.7590(3)	10.2238(2)	5.9932(1)	291.60(2)	1.00000	4.7624(6)	10.2260(3)	5.9936(2)	291.93(4)	1.00000
0.147(4)	4.7583(4)	10.2187(3)	5.9909(2)	291.30(3)	0.9990(1)	4.7624(6)	10.2209(3)	5.9914(2)	291.64(4)	0.9990(1)
0.748(4)	4.7532(5)	10.1974(3)	5.9813(2)	289.91(3)	0.9942(1)	4.7572(6)	10.2003(3)	5.9821(2)	290.29(4)	0.9944(1)
1.089(4)	4.7493(5)	10.1861(3)	5.9760(2)	289.10(3)	0.9914(1)	4.7544(7)	10.1883(3)	5.9767(2)	289.50(4)	0.9917(1)
1.619(5)	4.7455(5)	10.1674(3)	5.9675(2)	287.93(3)	0.9874(1)	4.7503(6)	10.1698(3)	5.9684(2)	288.33(3)	0.9877(1)
2.020(6)	4.7418(2)	10.1543(2)	5.9615(1)	287.04(1)	0.98436(5)	4.7461(6)	10.1561(3)	5.9625(3)	287.41(3)	0.9845(1)
3.314(8)	4.7314(3)	10.1130(2)	5.9424(2)	284.33(2)	0.97508(6)	4.7365(6)	10.1152(3)	5.9436(2)	284.76(3)	0.9754(1)
3.593(7)	4.7292(3)	10.1040(2)	5.9383(1)	283.75(2)	0.97309(6)	4.7341(6)	10.1066(2)	5.9396(2)	284.18(4)	0.9735(1)
3.929(7)	4.7267(3)	10.0941(2)	5.9337(1)	283.11(2)	0.97088(6)	4.7322(7)	10.0963(3)	5.9347(2)	283.55(4)	0.9713(1)
4.44(5)	4.7231(4)	10.0790(3)	5.9266(2)	282.13(2)	0.96750(8)	4.7288(6)	10.0813(2)	5.9279(2)	282.60(3)	0.9680(1)
5.35(2)	4.7164(4)	10.0524(3)	5.9142(2)	280.40(3)	0.96157(9)	4.7222(6)	10.0553(2)	5.9161(2)	280.91(4)	0.9623(1)
5.684(9)	4.7138(4)	10.0421(3)	5.9094(2)	279.73(3)	0.95929(9)	4.7190(8)	10.0448(3)	5.9111(3)	280.20(5)	0.9598(2)
7.104(8)	4.7041(1)	10.0050(3)	5.8916(1)	277.27(2)	0.95084(6)	4.7109(5)	10.0073(2)	5.8936(2)	277.84(3)	0.9517(1)

582 Table 3. Mode frequencies (in cm^{-1}), mode Grüneisen parameters, and mode assignments for observed Raman modes of hydrous
583 olivine $Fo_{97}Fa_3$ containing 4883 ppmw water (SZ0407A), with hydrous and anhydrous forsterite.

Hydrous $Fo_{97}Fa_3$ (This study)			Hydrous Fo_{100} (Hushur et al. 2009)		Anhydrous Fo_{100} (Chopelas 1991)		
Symmetry	Mode frequency	Mode Grüneisen Parameters	Mode frequency	Mode Grüneisen Parameters	Mode frequency	Mode Grüneisen Parameters	Mode type
A_g	227.0	0.88	228.4	0.689	226	0.674	SiO_4 translation
A_g	302.5	1.62	305.6	1.31	304	1.63	M2 translation
B_{2g}	325.2	1.65			323		Mix (M2 translation)
B_{2g}	368.9	1.37			365		Mix (SiO_4 rotation)
B_{3g}	432.9	1.82	435.7	1.51	435	1.4	Mix (SiO_4 rotation)
A_g	542.3	0.69	545	0.467	545	0.528	v_4
B_{2g}	588.4	0.85	588.7	0.481	592		v_4
A_g	606.9	1.01	608.2	0.732	608	0.704	v_4
A_g	823.1	0.77	824.4	0.582	824	0.483	v_1+v_3
A_g	854.5	0.655	856.2	0.426	856	0.489	v_1+v_3
B_{3g}	920.0	0.58	921		920	0.382	v_3
A_g	960.0	0.878	967	0.586	965	0.661	v_3

584

585

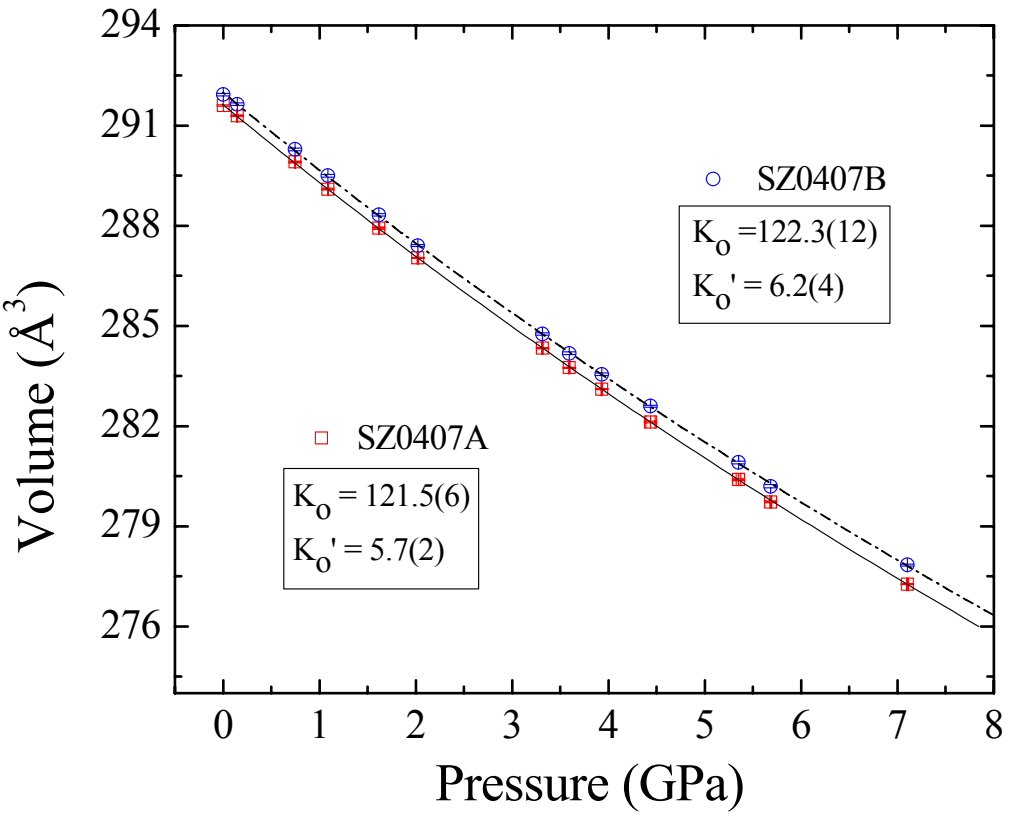

586

587 Figure 1. Unit-cell volumes of hydrous olivine $Fo_{97}Fa_3$ containing 4883 ppmw water
588 (SZ0407A, open squares) and hydrous olivine $Fo_{97}Fa_3$ containing 8000 ppmw
589 water (SZ0407B, open circles) as a function of pressure obtained from single-
590 crystal XRD studies. Error bars are also shown in figure. Solid and dashed lines
591 represent the two best-fit equations of state

592

593

594

595

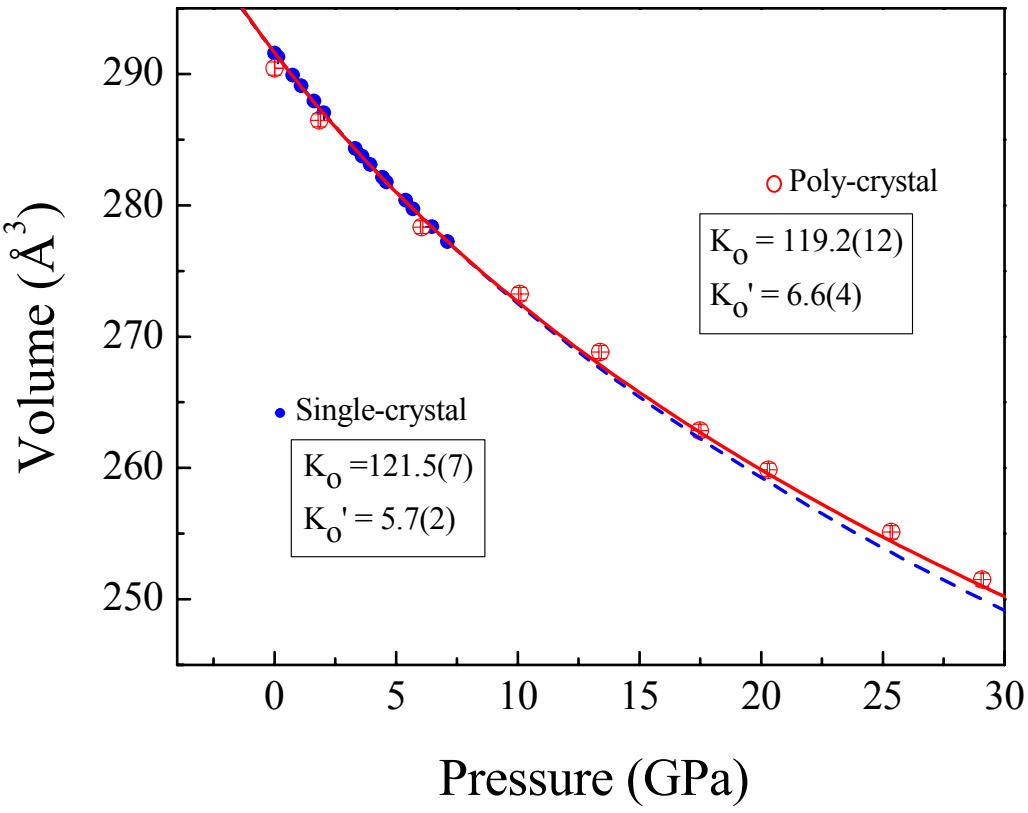

Figure 2. Unit-cell volumes of hydrous olivine $Fo_{97}Fa_3$ containing 4883 ppmw water (SZ0407A) as a function of pressure. Open symbols represent powder XRD data. Solid symbols are single-crystal XRD data. Solid and dashed lines represent the two best-fit equations of state, based on powder and single-crystal XRD, and single-crystal XRD respectively. Note that the symbols are larger than the uncertainties

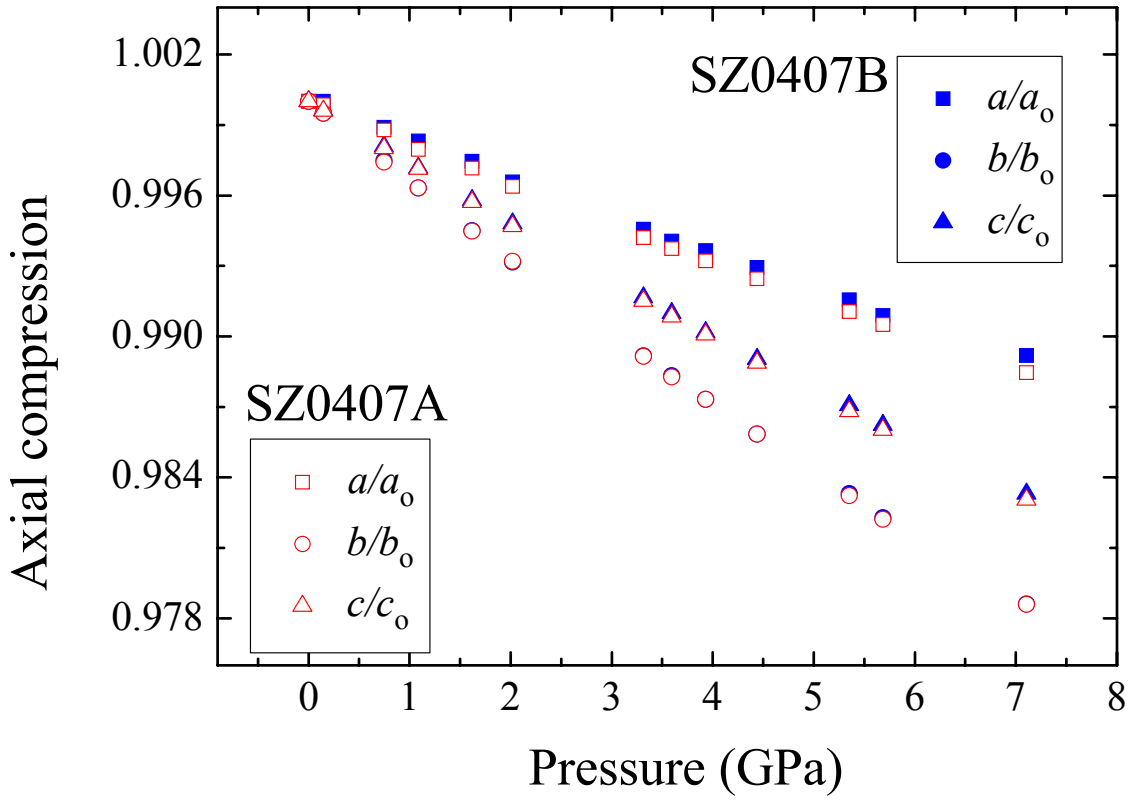

619

620

621

622 Figure 3. Axial compressions a/a_o, b/b_o and c/c_o as a function of pressure for a hydrous

623 olivine $Fo_{97}Fa_3$ containing 4883 ppmw water (SZ0407A) and for hydrous

624 olivine $Fo_{97}Fa_3$ containing 8000 ppmw water (SZ0407B). Note that the symbols

625 are larger than the uncertainties

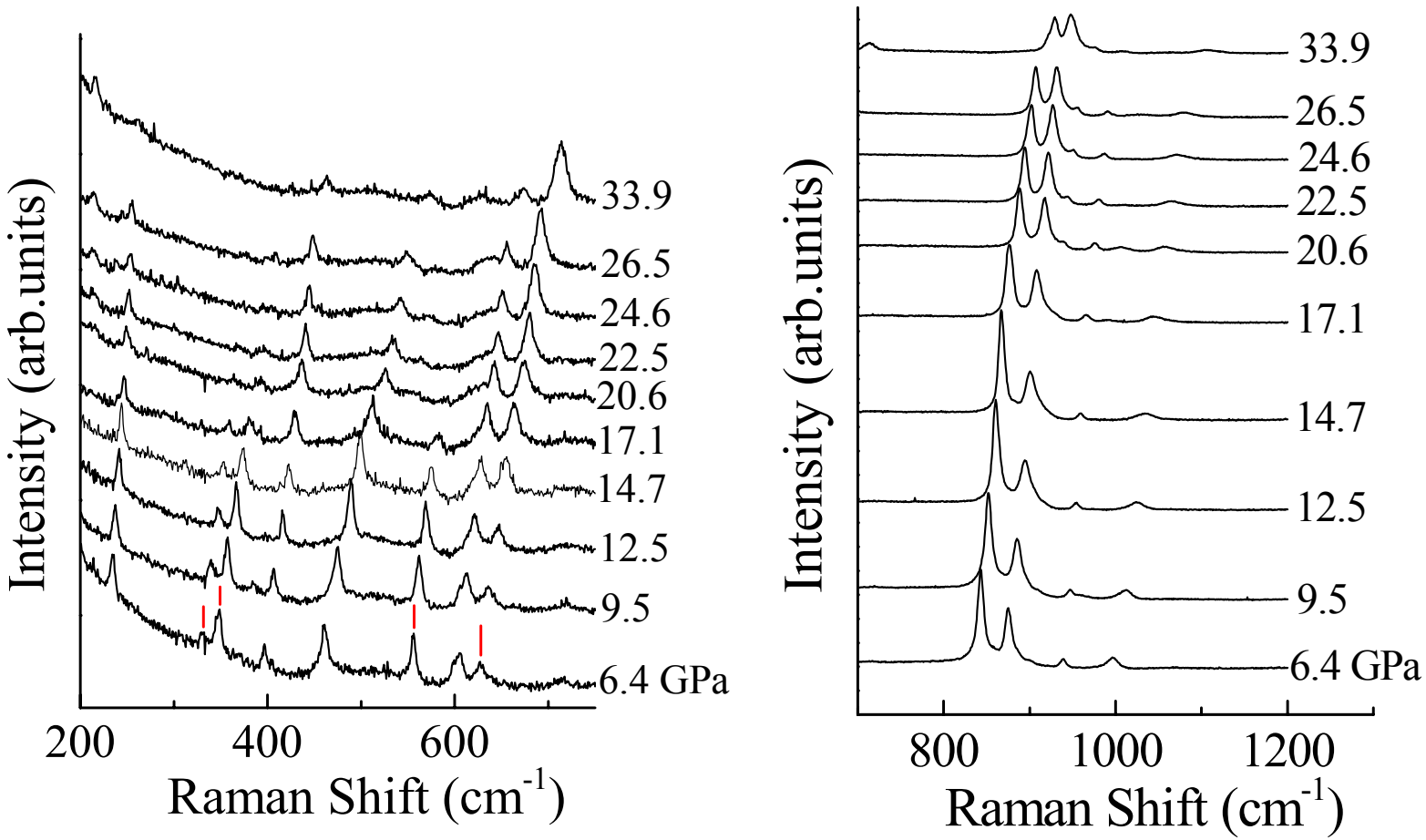

Figure 4. Raman spectra of hydrous olivine $Fo_{97}Fa_3$ containing 4883 ppmw water (SZ0407A) to 33.9 GPa.

635
636
637

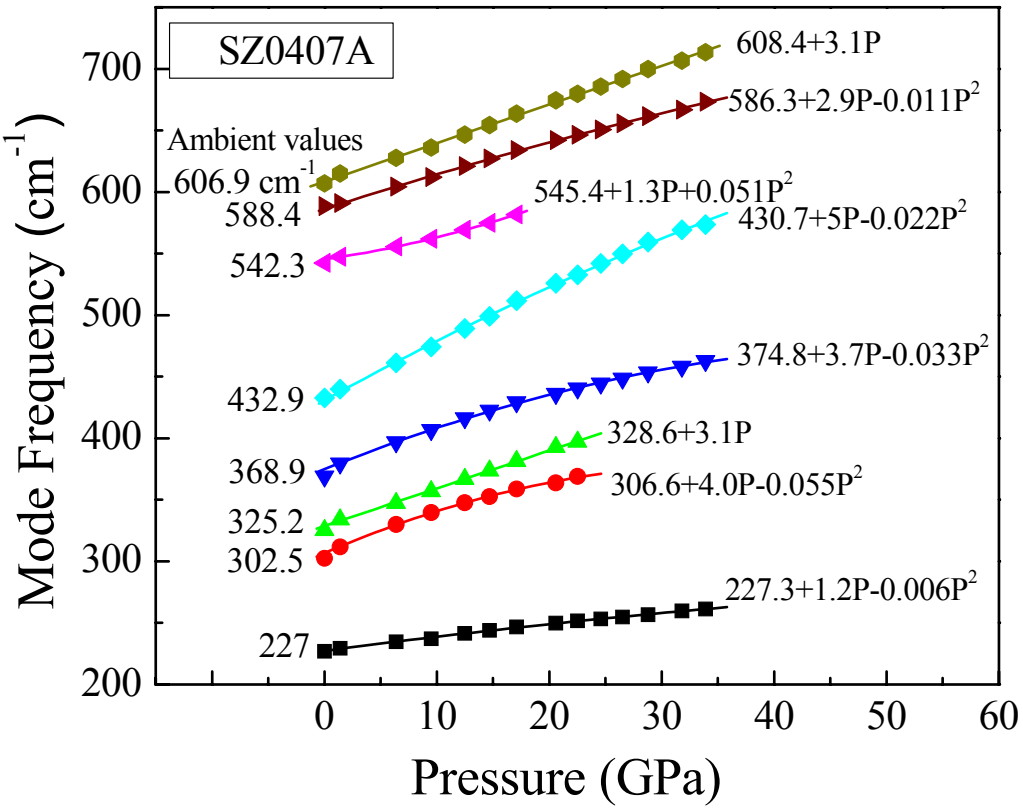

638

639 Figure 5. Pressure dependences of the observed low frequency Raman modes for hydrous
640 olivine $Fo_{97}Fa_3$ containing 4883 ppmw water (SZ0407A) from 200 ~ 750 cm^{-1}.

641
642
643
644
645

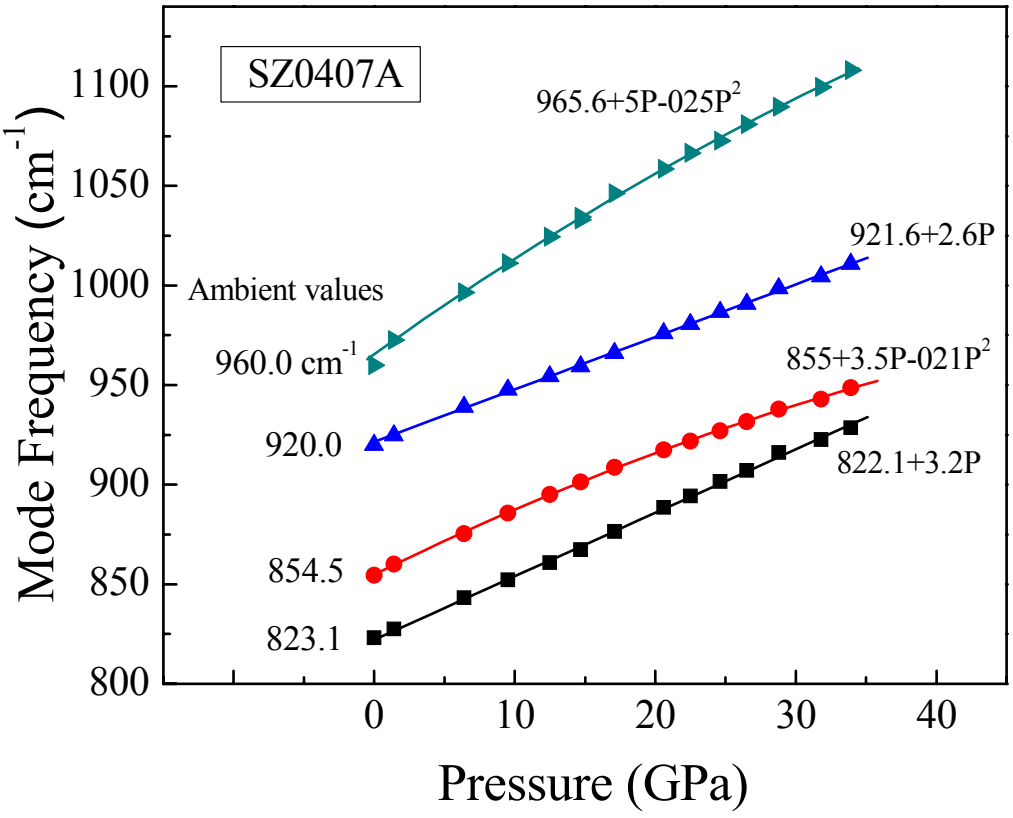

Figure 6. Pressure dependences of the four high frequency Raman modes for hydrous olivine $Fo_{97}Fa_3$ containing 4883 ppmw water (SZ0407A) from 800 ~ 1200 cm^{-1}.

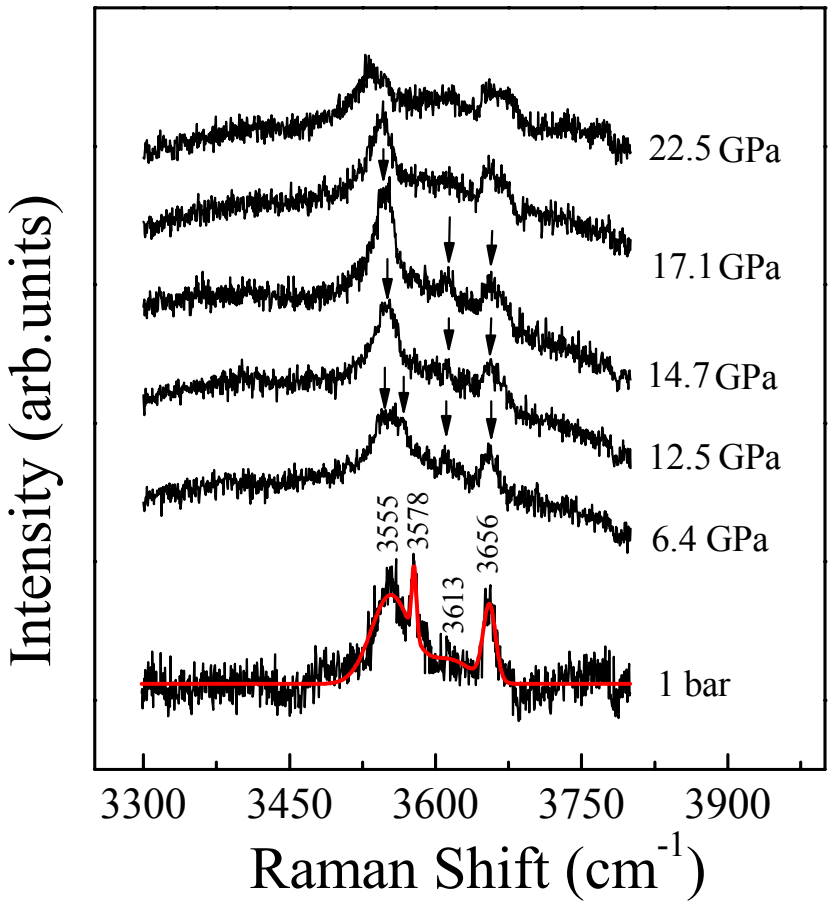

Figure 7. Pressure dependence of Raman spectra of hydrous olivine Fo97Fa3 containing 4883 ppmw water (SZ0407A) in the OH-stretching region. The spectra are offset for clarity. The solid red line in the 1 bar spectrum is a fit using four Gaussian. Labels at right side indicate pressure in gigapascals and numbers on the 1 bar spectrum indicate O-H stretching mode frequencies obtained from the fit.

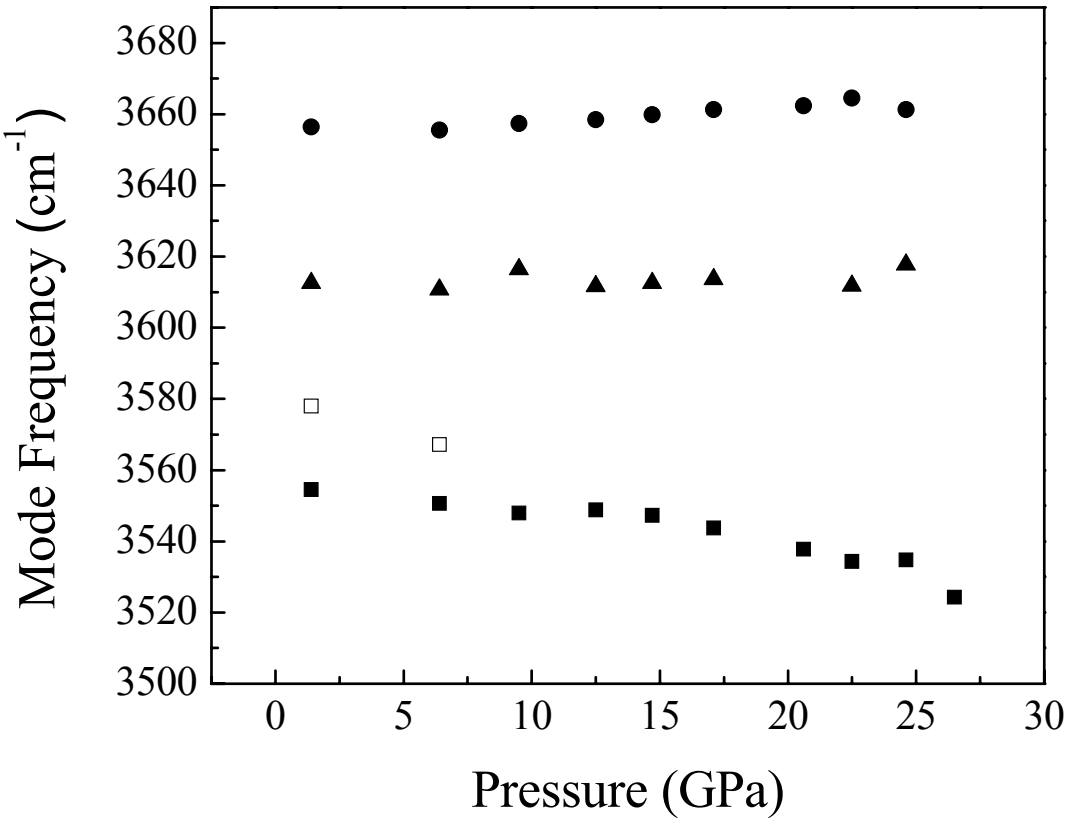

669

670 Figure 8. Pressure dependence of the Raman modes of hydroxyl group in hydrous olivine
671 $Fo_{97}Fa_3$ containing 4883 ppmw water (SZ0407A).

672

673

674

675